Toxicology and Applied Pharmacology 377 (2019) 114626

Contents lists available at ScienceDirect

Toxicology and Applied Pharmacology

journal homepage: www.elsevier.com/locate/taap

Microcystin-LR promotes necroptosis in primary mouse hepatocytes by overproducing reactive oxygen species

Yun-Li Wu[a,1], Yun He[b,1], Jia-Jian Shi[b], Tian-Xiu Zheng[a], Xin-Jian Lin[a], Xu Lin[a,b,*]

[a] Key Laboratory of Gastrointestinal Cancer (Fujian Medical University), Ministry of Education, School of Basic Medical Sciences, Fujian Medical University, Fuzhou, China
[b] Fujian Key Laboratory of Tumor Microbiology, Department of Medical Microbiology, Fujian Medical University, Fuzhou, China

ARTICLE INFO

Keywords:
Microcystins
Cyanbacteria
Eutrophication
Necroptosis
Apoptosis
Liver injury

ABSTRACT

Microcystin-LR (MC-LR) is a type of cyclic heptapeptide toxin produced by cyanobacteria during bloom events. MC-LR-induced cell death is critically involved in its potent specific hepatotoxicity. Many studies have demonstrated that prototypical apoptosis as a form of programmed cell death after MC-LR is associated with liver injury. However, whether another form of programmed cell death exists and the underlying mechanism have not been reported. Here, we demonstrate that MC-LR can induce necroptosis via ROS overactivation in primary mouse hepatocytes. Various potential pathways of programmed cell death induced by MC-LR were evaluated by annexin V/PI dual staining for flow cytometric analysis, image-based PI staining analysis and western blot analysis. Cell viability was determined by the CCK8 assay. Rupture of the plasma membrane was indicated by lactate dehydrogenase release. ROS was evaluated with the carboxy-H2DCFDA fluorescent probe. It was found that in MC-LR-treated cells, as the plasma membrane was damaged, annexin V/PI-stained double-positive cells were significantly induced and PI-stained nuclei were more diffuse. Western blot analysis showed that MC-LR treatment significantly upregulated the expression of necroptotic and apoptotic proteins. Mechanistically, MC-LR induced ROS overproduction by dysregulating the expression and activity of the pro-oxidants SOD1, MAOA, and NOX4 and the antioxidant GPX1. These results indicate the presence of a novel mechanism for MC-LR-mediated liver injury and present a novel target in the treatment of MC-LR-exposed patients.

1. Introduction

In recent years, due to serious eutrophication of freshwater, cyanobacterial blooms in aquatic environments have increased all over the word (Lone et al., 2017; Shuai et al., 2017). Accumulating evidence shows that toxins produced by cyanobacteria are responsible for various fatalities in animals and humans (Falconer and Humpage, 2005; Gehringer, 2004). Cyanobacteria (blue-green algae) are capable of producing a wide range of toxins including hepatotoxins, neurotoxins, cytotoxins, dermatoxins and irritant toxins (lipopolysaccharides) (Amado and Monserrat, 2010). Among these cyanotoxins, the cyclic heptapeptide toxins microcystins (MCs) are the most commonly occurring and the most widely studied natural toxins (Bischoff, 2001). More than 90 isoforms of MCs have been detected, among which microcystin-LR (MC-LR) is the most ubiquitous and toxic (Campos and Vasconcelos, 2010), and is classified as a type II B potential carcinogen by the International Agency for Research on Cancer. Aquatic organisms are particularly at risk of exposure to MCs, which can come into the direct contact of organisms after the senescence and lysis of cyanobacterial cells. In addition, some phytoplanktivorous and omnivorous species ingest cyanobacterial cells as food (Amado and Monserrat, 2010; Huang et al., 2015). This leads to the bioaccumulation of MCs in aquatic animals and their entry into the food chain, where they pose a health risk to livestock and human beings (Jia et al., 2014; Song et al., 2007). MCs are able to induce a series of liver injuries, including acute liver failure and primary liver cancer (Pouria et al., 1998; Soares et al., 2006; Zegura et al., 2011). Humans can be exposed to MCs through several routes: the oral one is the most important by far, and it occurs via ingestion of contaminated drinking water or food (including dietary supplements). In addition, dermal/inhalation exposure occurs through the domestic use of water (i.e., during a shower) or with professional and recreational activities (i.e., fishing). At present, the exact mechanisms of MC-induced hepatotoxicity and tumor promotion activity have not been fully elucidated.

* Corresponding author at: Key Laboratory of Gastrointestinal Cancer (Fujian Medical University), Ministry of Education, School of Basic Medical Sciences, Fujian Medical University, 1 Xue Fu North Road, University Town, Fuzhou, Fujian 350122, China.
E-mail address: linxu@mail.fjmu.edu.cn (X. Lin).
[1] Both authors contributed equally to this study.

https://doi.org/10.1016/j.taap.2019.114626
Received 24 March 2019; Received in revised form 31 May 2019; Accepted 11 June 2019
Available online 12 June 2019
0041-008X/

Critical to preventing MC-LR-induced liver injury is understanding the molecular basis behind MC-LR-induced hepatocyte cell death. The current literature largely focuses on apoptosis as a form of programmed cell death after MC-LR-induced liver injury (Chen and Xie, 2016; Ding et al., 2000; Kleppe et al., 2015). This hypothesis has been extensively tested in primary rat hepatocytes, and transfected cell models (Ding et al., 2000; Komatsu et al., 2007; Takumi et al., 2010). However, Fladmark et al. reported that the mammary carcinoma cell line MCF-7 with a defective caspase-3 enzyme, which is highly resistant to pan-caspase inhibitor *Z*-VAD-fmk-induced apoptosis, is sensitive to MC-LR-induced cell death (Fladmark et al., 1999). This finding indicates that MC-LR induces cell death in this cell line through a mechanism other than apoptosis. Whether another form of programmed cell death in addition to apoptosis might exist in MC-LR-treated cells still needs to be investigated.

Necroptosis and pyroptosis have been characterized as the two main types of lytic programmed cell death (Zhang et al., 2018). Necroptosis occurs in a caspase-independent manner, and the morphological features of necroptotic cells (including early membrane integrity, cell and intracellular organelle swelling) more closely resembles those of classical necrosis than apoptosis. Crucial to necroptosis is the activation of both receptor-interacting protein (RIP) 1 and RIP3; phosphorylation of MLKL by RIP3 leads to MLKL oligomerization and, subsequently, the disruption of plasma membrane integrity (Cai et al., 2014; Cho et al., 2011; Cho et al., 2009; Sun et al., 2012; Zhang et al., 2009). On the other hand, pyroptosis is dependent on caspase activity; this pathway is initiated by inflammasomes, which activate caspase-1 or caspase-11/4/5 to cleave gasdermin D (GSDMD) or activate caspase-3 to cleave gasdermin E (GSDME). The N-terminal pore-forming domain of GSDMD or GSDME undergoes oligomerization to form nonselective pores in the membrane that drive cell swelling and membrane rupture, leading to pyroptosis (Ding et al., 2016; Wang et al., 2017). Thus, presumably, MC-LR might induce cell death via necroptotic or pyroptotic pathways.

In the present study, in order to understand the alternative mechanisms by which MC-LR induces cancer cell death, we examined the expression and concentrations of necroptosis- and pyroptosis-associated factors in primary cultured mouse hepatocytes subjected to MC-LR-induced hepatotoxicity and cell injury. This is the first study to investigate the possible involvement of necroptosis and pyroptosis in the cell death mechanisms of MC-LR in hepatocytes. We believe that our findings have value from a therapeutic perspective, as identifying the programmed cell death pathways involved will help determine future targets for liver injury and associated diseases.

2. Materials and methods

2.1. Isolation and culture of mouse hepatocytes

The primary cultured mouse hepatocytes were isolated and purified from a 28-day-old male C57BL/6 mouse with the modified two-step perfusion method. An anaesthetized mouse liver was perfused with calcium and magnesium-free Krebs-Ringer buffer containing collagenase IV (Sigma Aldrich, St. Louis, MO, USA). The primary isolated mouse hepatocytes were washed extensively with Dulbecco modified Eagle medium (DMEM) to remove fibroblasts and liver non-parenchymal cells. The hepatocytes were then plated onto collagen-coated plates coated with DMEM (Gibco BRL, Grand Island, NY, USA) supplemented with 10% fetal bovine serum (FBS; PAN-Biotech GmbH, Adenbach, German) and penicillin (50 IU/m) and streptomycin (50 μg/ml, Gibco). All animal experiments were performed in accordance with the animal protocols and regulations of the FJMU Experimental Animal Ethics Committee of Fujian Medical University (Fuzhou, Fujian, China).

2.2. MC-LR treatment

The human hepatoma cell line HepG2 (HB-8065, ATCC, Manassas, VA, USA) and mouse hepatoma cell line Hepa 1–6 (SCSP-512, Stem Cell Bank, Chinese Academy of Sciences) were maintained in DMEM, supplemented with 10% (*v*/v) FBS. The cyanobacterial toxin MC-LR used in the toxicity assays was purchased from Enzo Biochem (NY, USA), and the purity was demonstrated to be 90–99% (HPLC analysis). The cells were allowed to grow for 24 h and subsequently treated with freshly prepared MC-LR (diluted in DMEM containing 10% FBS and 1% antibiotics) at concentrations ranging between 0 and 10 nM for primary cultured mouse hepatocytes, 20 μM for HepG2 and 10 μM for Hepa 1–6. DMEM without MC-LR served as the negative control. In some experiments, z-VAD-fmk (5 μM, V116; Sigma), a potent pan-caspase inhibitor; necrostatin-1 (nec-1) (N9037, 8 μM; Sigma), a specific inhibitor of RIP1; mtROS scavenger Mito-tempo (3 μM); total ROS scavenger N-Acetyl-L-cysteine (NAC, sigma, A7250, 5 mM) or vehicle control was added 1 h prior to the addition of MC-LR.

2.3. Periodic acid-Schiff staining

Hepatocytes synthesize glycogen, which can be identified by periodic acid/Schiff (PAS) staining. Hepatocytes grown on glass cover-slips were fixed with Carnoy fixative and stained with periodate solution for 10 min. Following hematoxylin staining, the cover-slips were dried and photographed with a microscope camera (Olympus, Tokyo, Japan).

2.4. Immunohistochemical analysis

Immunohistochemical evaluation of hepatocytes for cytokeratin 18 (CK18) expression was performed. Hepatocytes were seeded on glass cover-slips and fixed with 4% paraformaldehyde for 30 min. Following this, endogenous peroxidase activity was quenched by incubation with 3% hydrogen peroxide. Subsequently, the sections were incubated with anti-cytokeratin 18 (1:1500; Abcam, Cambridge, UK) for 1 h at room temperature, and this was followed by labeling with horseradish peroxidase-conjugated secondary antibody for 30 min at room temperature. Diaminobenzidine was applied as the chromogenic substrate, and hematoxylin, as the nucleus counterstain. The results were examined under a light microscope (Olympus IX71). Immunohistochemical assessment was performed based on the prevalence and intensity of brown granules.

2.5. Lactate dehydrogenase assay

MC-LR-induced lactate dehydrogenase (LDH) leakage was determined by the LDH cytotoxicity assay kit (Roche Diagnostics, Basel, Swiss) according to the manufacturer's instructions. Briefly, after MC-LR exposure and the indicated treatment, the cells were lysed and the supernatants and culture medium were collected to detect LDH release. Absorbance values were monitored with a microplate reader (BioTek) at 490 nm, and the percentage of LDH release was calculated.

2.6. Cell viability assay

Cell proliferation and survival were assessed using Cell Counting Kit-8 (CCK-8; Dojindo, Kuma-moto, Japan), as described by the manufacturer. Cells were seeded at a density of 5×10^3 cells per well in 96-well plates and incubated for 24 h to induce adhesion. After 24 h, MC-LR was added to the medium at the indicated concentrations. The cells were then cultured for another for 12, 24, 48, 72, 96 or 120 h. Then, 10 μl of CCK-8 working solution was added into each well and incubated at 37 °C for 0.5 h. Absorbance at 450 nm was measured using a microplate reader (BioTek).

2.7. Flow cytometry analysis

To examine the morphological features of apoptotic and necrotic cells, the cells were seeded in the 12-well plate format (Nunc Products,

Thermo Fisher Scientific Inc.) at 40% confluency and subjected to the indicated treatments. The cells were then collected, washed with PBS twice and stained using the FITC Annexin V apoptosis detection kit (BD Biosciences, NY, USA) according to the manufacturer's instructions. The stained cells were analyzed with flow cytometry (FACSVerse, BD Biosciences) using the FACSuite software (BD Biosciences). Apoptotic cells were identified by annexin V staining, while necroptotic and pyroptotic cells were identified by PI staining.

2.8. Microscopic imaging of cell death

To examine cell death, primary mouse hepatocytes were treated as indicated in 35-mm glass bottom dishes for image capture. PI (5 ng/ml) was added to the medium for monitoring cell membrane integrity. Static bright field images of dead cells were captured using a confocal microscope (Leica TCS SP8; Leica, Heidelberg, Germany) at room temperature. The images were processed using the NIH Image J software with the commercially available.

2.9. Activity analysis

Caspase-3 or −9 activity was determined using a caspase-3 or caspase-9 activity assay kit (Beyotime Institute of Biotechnology, Jiangsu, China) according to the manufacturer's instructions. Briefly, after 2.5 nM MC-LR treatment, cells were lysed and the supernatant was used to detect the activity of caspase-3 or −9. The adsorption values were obtained at 405 nm with a microplate reader.

The enzymatic activity of SOD1, MAOA, NOX1 and GPX1 was measured using an assay kit, according to the manufacturer's protocol (Nanjing Jiancheng Bioengineering Institute, Nanjing, China). The protein concentration in the cell lysate was determined using the BCA method to normalize enzymatic activity. The assay results are expressed as the unit of enzymatic activity per milligram of protein (U/mg protein).

2.10. Measurement of intracellular ROS level

ROS detection was performed with an Image-iT LIVE green reactive oxygen species detection kit (I36007; Molecular Probes, Eugene, OR) in accordance with the manufacturer's instructions, Briefly, primary cultured hepatocytes were seeded in 35-mm dishes at a density of 1×10^5. Following this, 25 μM of carboxy-H2DCFDA was added at 48 h after MC-LR treatment and incubated for 30 min. After counterstaining with Hoechst 33342, the cells were visualized under a confocal microscope (Leica, Heidelberg, Germany). The intracellular ROS appeared green, and the green fluorescence intensity was calculated.

2.11. Determination of intracellular glutathione content

The intracellular glutathione (GSH) levels were measured with a glutathione assay kit (Sigma). Briefly, 1×10^8 cells were harvested and resuspended in three volumes of 5% 5-sulfosalicylic acid. The suspension was then snap frozen in liquid nitrogen and thawed at 37 °C twice. All the samples were centrifuged at 10,000*g* for 10 min, and 10 μl of each supernatant was assayed spectrophotometrically according to the manufacturer's instructions. Absorbance was measured using a microplate reader (BioTek) set to 412 nm.

2.12. RNA extraction and quantitative real-time PCR

Total RNA was extracted from MC-LR-treated cells with TRIzol reagent (Invitrogen), in accordance with the manufacturer's instructions. The reverse transcription reaction was carried out with 2 μg of RNA by using the PrimeScript RT-PCR Kit (TaKaRa, Japan) in accordance with the manufacturer's recommendations. Quantitative real-time PCR (qPCR) was performed with the Agilent Mx3000P Real-Time PCR System (Agilent Technologies, Santa Clara, CA) and the SYBR Premix Ex Taq Kit (TaKaRa) in accordance with the manufacturer's instructions. GAPDH served as an internal control. Each sample was measured in triplicate. The relative mRNA levels of CAT, SOD1, SOD2, SOD3, GSR, GSTT2, NOX4, NQO1, MAOA, UCP2, NOS3, GPX3, GPX1, and GCLC were calculated by normalization to endogenous GAPDH mRNA expression prior to comparative analysis with the $2^{-\Delta\Delta Ct}$ method. The primers used are listed in Table 1.

Table 1
List of primers used in the study.

Oligonucleotides		Sequences (5′ → 3′)	Product size (bp)
CAT	Forward	GCCAATGGCAATTACCCGTC	277
	Reserve	GAGTGTCCGGGTAGGCAAAA	
SOD1	Forward	GGAACCATCCACTTCGAGCA	136
	Reserve	CTGCACTGGTACAGCCTTGT	
SOD2	Forward	AGAACCCAAAGGAGAGTTGCT	158
	Reserve	AGGCAGCAATCTGTAAGCGA	
SOD3	Forward	TGCTGCTCGCTCACATAACA	144
	Reserve	GAGGTTCTCTGCACCTGTCA	
GSR	Forward	TGGCACTTGCGTGAATGTTG	233
	Reserve	CGAATGTTGCATAGCCGTGG	
GSTT2	Forward	CCTCAGCCCTGCTTTTGGTAT	296
	Reserve	TCATGTGCTGCCCTTTGAGTA	
NOX4	Forward	CCAAATGTTGGGCGATTGTGT	219
	Reserve	GGCTACATGCACACCTGAGA	
NQO1	Forward	AGCCAATCAGCGTTCGGTAT	237
	Reserve	TCGAGTCCTTCAGCTCACCT	
GPX3	Forward	CCAATACCTTGAACTGAATGCAC	206
	Reserve	GCTCTTTCTCCCCGTTCACA	
GPX1	Forward	CAGTTCGGACACCAGGAGAA	154
	Reserve	TCCGCAGGAAGGTAAAGAGC	
GCLC	Forward	TTGGGTCGCAAGTAGGAAGC	283
	Reserve	GGTCTCTTCCCAGCTCAGTG	
MAOA	Forward	ATCTCAGGATTGGCTGCTG	183
	Reserve	TTCTGTTCTGGGTTGGTCC	
UCP2	Forward	TCCACGCAGCCTCTACAAT	257
	Reserve	CAGTGCTCTGGTATCTCCGA	
NOS3	Forward	CTTCGTTCGGTTGACCAA	172
	Reserve	AGCAGGATGCCCTAACTACC	
GAPDH	Forward	TGCACCACCAACTGCTTAGC	218
	Reserve	AGCTCAGGGATGACCTTGCC	

2.13. Western blot analysis

A total of 30 μg protein was subjected to 10% sodium dodecyl sulfate-polyacrylamide gel electrophoresis, and the gels were electrophoretically transferred to a polyvinylidene fluoride membrane (Millipore, Billerica, MA). Protein blots were incubated separately with the following primary antibodies: anti-GSDMD (ab225867) and anti-GSDME (ab223877) from Abcam Biotechnology, and anti-caspase 3 (#9662), anti-caspase 9 (#9504), anti-PARP (#9542), anti-RIP1 (#9493), anti-RIP3 (#95702), anti-MLKL (#37705), anti-phospho-MLKL (#37333) and anti-GAPDH (#2118) from Cell Signaling Technology. Next, the corresponding alkaline phosphatase-conjugated secondary antibodies were added. The bands were scanned using ImageQuant LAS 4000 mini (GE Healthcare, Waukesha, WI, USA). The intensity of the band signals was quantified using the densitometric software Quantity One (BioRad, Hercules, CA, USA). GAPDH served as an internal control.

2.14. Expression vectors construction and RNA interference assay

pCDNA3.1-GPX1 was constructed by ligation of the mouse GPX1 cDNA into the *Xho*I and *Kpn*I sites of the pcDNA3.1(−)/myc-His A (Invitrogen, Carlsbad, CA). GPX1 cDNA was synthesized by Anhui General Biosystems Co.,Ltd. MAOA-specific small interfering RNA (siRNA) mix (No. sc-35848), NOX4 siRNA mix (No. sc-41587) and

SOD1 siRNA mix (No. sc-36522) were obtained from Santa Cruz Biotechnology, and NC-siRNA, a nontargeting siRNA, was used as a negative control. 48 h after transfection the cells were harvested for Western blot analysis, or Flow cytometry analysis.

2.15. Statistical analysis

All data were presented as the mean ± standard deviation (SD). An unpaired *t*-test was used to analyze the differences between the different groups and the control group with the GraphPad Prism 7.0 software. A p value of < 0.05 was considered to indicate statistical significance.

3. Results

3.1. Induction of programmed cell death by MC-LR

In the present study, primary cultured mouse hepatocytes were used to systematically investigate the hepatotoxic characteristics of MC-LR. The purity of the isolated mouse hepatocytes, as determined by CK18 immunohistochemical and PAS staining, was > 95% in all cases after 24 h of incubation (Fig. 1a and b). Considered in combination with cell morphology, cells were used for the experiments after 24 h of culture.

To determine the non-cytotoxic concentration range of MC-LR, we performed a dose-response analysis with freshly isolated primary mouse hepatocytes by the CCK8 assay. MC-LR was added at a concentration range of (0–100 nM) for 48 h, and the obvious dose-response curve was obtained (Fig. 1c). The IC_{50} values, calculated from the curve, showed that the 48 h IC_{50} values of MC-LR in primary mouse hepatocytes was 26 nM. These data indicate that primary mouse hepatocytes are highly sensitive to MC-LR treatment, and MC-LR induces cytotoxicity when its concentration reaches a certain level. For subsequent experiments, MC-LR was not used at concentrations above 10 nM was the highest concentration tested for MC-LR.

In order to investigate the induction of programmed cell death by MC-LR (Fig. 1d), Annexin V/PI dual staining for flow cytometric analysis was used to determine the level of apoptosis. As shown in Fig. 1e, apoptosis was induced in MC-LR-treated cells, as a dose-dependent increase in annexin V-positive staining without PI uptake was observed (1.53%–12.50%, lower right quadrant). Further, MC-LR administration also led to a significant dose-dependent increase in the annexin V and PI double-positive cells (1.52%–15.19%, upper right quadrant). In the case of annexin V and PI double staining, it is not possible to distinguish between secondary necrotic/late apoptotic and necrotic cells using the classical flow cytometry analysis. Inducing of apoptosis by MC-LR has been extensively studied, but whether other forms of programmed cell death in addition to apoptosis might exist in MC-LR-treated cells still needs to be investigated.

To distinguish between late apoptotic and necrotic cells, image-based analysis of Annexin V/PI staining was performed. As shown in Fig. 1f, the MC-LR-treated cells exhibited diffuse PI staining, and thereby, a very intense fluorescence signal all over the nuclear area on account of the swollen necrotic nuclei; this was different from the small areas of high PI intensity observed on account of the condensed chromatin present at the late apoptotic/secondary necrosis stage. Furthermore, the viability of cells dropped significantly upon MC-LR stimulation (Fig. 1g); notably, the concentration of released LDH, which is an indicator of plasma membrane rupture, was observed at a concentration above 5 nM (Fig. 1h). These data together indicate that MC-LR induces various types of programmed cell death, in addition to apoptosis, in primary mouse hepatocytes.

3.2. Induction of necroptosis by MC-LR in primary mouse hepatocytes

MC-LR is known to induce cell death in primary hepatocytes by caspase-3-dependent apoptosis pathways (Fladmark et al., 1999). In our study, as expected, primary mouse hepatocytes treated with MC-LR showed marked cleavage of the pro-apoptotic proteins caspase-3 and caspase-9 and the caspase substrate PARP, which is concurrent with the activation of caspase-3 and -9 (Fig. 2a-c).

Necroptosis and pyroptosis have been characterized as the two main types of programmed necrosis pathways (Zhang et al., 2018). GSDMD and GSDME were recently identified as key executors of pyroptosis (Shi et al., 2015), so we investigated whether they are involved in MC-LR-induced cell death. As shown in Fig. 2d-e, primary mouse hepatocytes treated with MC-LR did not exhibit cleavage of pyroptotic GSDMD or GSDME. This indicates that the programmed cell death mechanism of MC-LR does not involve pyroptosis. On the other hand, when we examined the proteins associated with necroptosis, we found high levels of RIP1, RIP3 and MLKL expression in the MC-LR-treated cells as compared with the controls (Fig. 2f). RIP3-dependent signaling may also mediate apoptosis (Dondelinger et al., 2013; Newton et al., 2014), and it has been shown to directly regulate inflammatory signaling (Vince et al., 2012). Therefore, in order to verify the findings, we evaluated the expression of p-MLKL, a non-redundant executer of necroptosis, in primary mouse hepatocytes by western blot analysis. The p-MLKL levels were also substantially increased after MC-LR treatment, in comparison with the control cells (Fig. 2f). Notably, the p-MLKL and MLKL expression levels increased by 2.7- and 1.6-fold, respectively, in MC-LR-treated cells; this is further indicative of MLKL phosphorylation (Fig. 2g). Furthermore, necrostatin-1 (nec-1), a specific inhibitor of RIP1, significantly reduced the number of PI + cells (Fig. 3a). The results of western blot analysis also demonstrated that the expression of RIP1, RIP3, MLKL and p-MLKL was significantly inhibited by nec-1 (Fig. 3b). On the other hand, z-VAD, a pan-caspase inhibitor, only downregulated the number of annexin V–FITC + cells, but did not affect the number of PI + cells after MC-LR treatment (Fig. 3a and c). Further, co-treatment with both z-VAD and nec-1 resulted in a reduction in the number of PI + cells and annexin V–FITC + cells (Fig. 3c). Moreover, nec-1 significantly reduced LDH release, but z-VAD did not have the same effect in MC-LR-treated cells (Fig. 3d). The decrease in the cell viability of MC-LR-treated cells was significantly inhibited by nec-1 and z-VAD (Fig. 3e). Similar results were obtained with mouse hepatoma cell line Hepa 1–6 (Fig. 4a-c) and human hepatoma cell line HepG2 (Fig. 4d-f) treated with MC-LR at 20 μM (HepG2) or 10 μM (Hepa 1–6). These results indicate that MC-LR induced programmed cell death in primary mouse hepatocytes and hepatoma cell lines via necroptosis too (in addition to apoptosis).

3.3. Role of ROS in MC-LR-induced necroptosis in primary mouse hepatocytes

Excessive levels of ROS have been reported to be associated with apoptotic or necroptotic cell death (Dixon and Stockwell, 2014; Schieber and Chandel, 2014). Further, previous studies have shown that excessive production of ROS and oxidative damage plays a significant role in MC-LR-induced toxicity and apoptosis (Gates et al., 2003; Huang et al., 2015; Jayaraj et al., 2006; Shammo and Stein, 2016). Therefore, in this study, we investigated the role of ROS in MC-LR-induced programmed cell death. First, we examined the intracellular levels of total GSH, a major intracellular antioxidant and indicator of ROS accumulation, in the control and MC-LR-treated cells, and we found that MC-LR exposure resulted in a significant drop in GSH (Fig. 5a). Next, to determine whether MCLR-induced cell death is caused by intracellular oxidative stress, carboxy-H2DCFDA was used as a probe to monitor the ROS levels during live cell imaging. As shown in Fig. 5b and c, MC-LR-treated cells produced considerably more ROS than control cells. We tried to determine whether the increased ROS levels induced by MC-LR were associated with changes in the levels of pro-oxidant/antioxidant enzymes; therefore, the expression of 14 pro-oxidant/antioxidant enzymes [CAT (Deng et al., 2012; Yabe et al., 2002), SOD1 (Iuchi et al., 2007), SOD2 (Hosoki et al., 2012), SOD3 (Kwon et al., 2015), GSR (Han

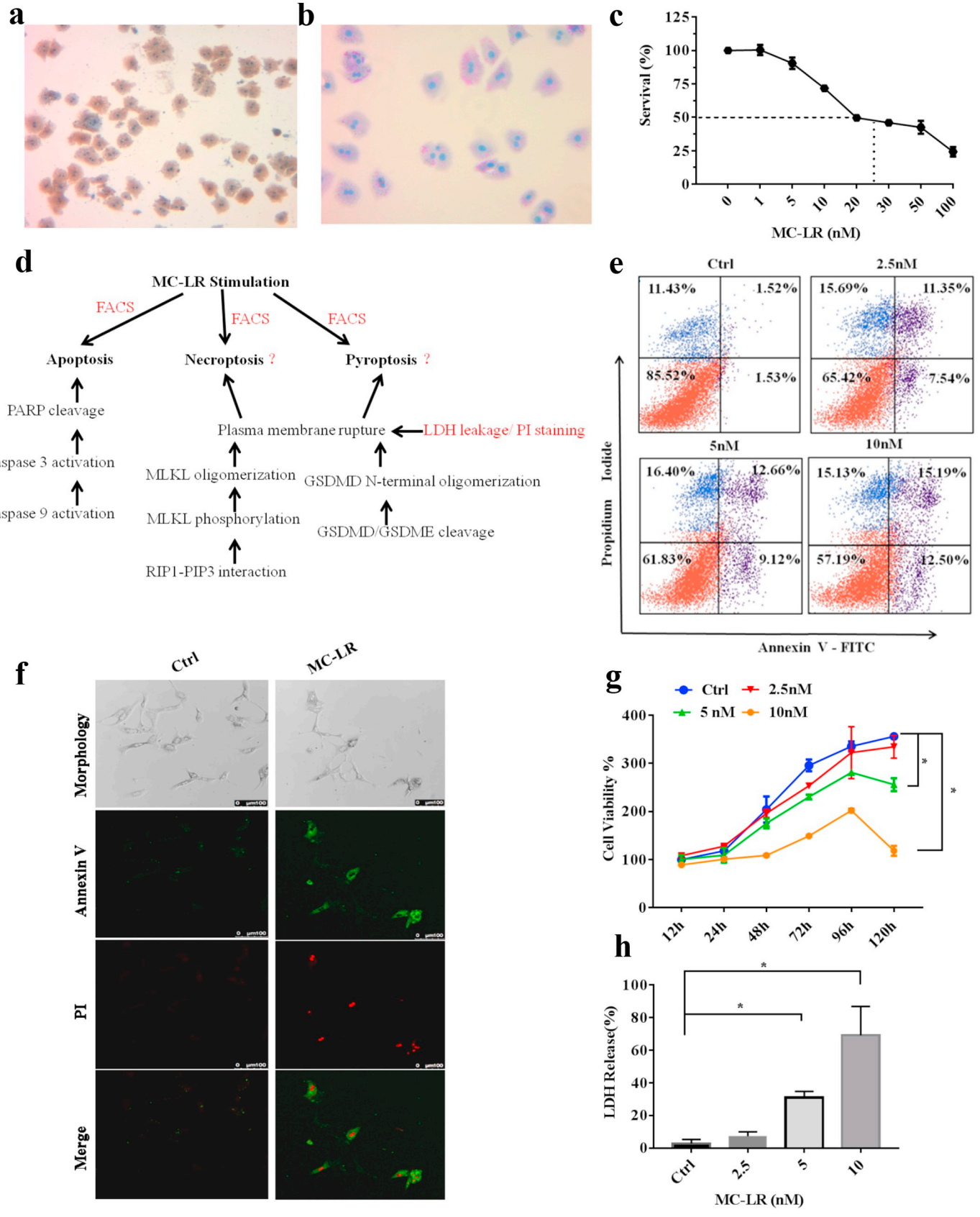

(caption on next page)

Fig. 1. MC-LR-induced cell death in primary mouse hepatocytes.
(a and b) Hepatocytes were isolated from 28-day-old C57BL/6 mice, and assessed after PAS (a) and IHC (b) staining. (c) The 48-h IC_{50} assay showed that the minimum 50% inhibitory concentration of MC-LR in primary mouse hepatocytes is about 26 nM. (d) Schematic illustration of the screening strategy for different forms of programmed cell death. (e) Flow cytometry analysis of propidium iodide (PI) and annexin V–fluorescein isothiocyanate (FITC)-stained cells treated with 2.5–10 nM MC-LR. (f) Representative confocal imaging of cells treated with 2.5 nM MC-LR. Cell morphological features were visualized by phase-contrast imaging (upper panel), and cell integrity was monitored by annexin V–FITC and PI uptake (lower panel). (g and h) Detection of cell viability and LDH release in cells treated with different concentrations of MC-LR. DMEM treatment served as the negative control. All data are shown as the mean ± SD values from three separate experiments performed in duplicate. *$p < .05$ versus the control cells.

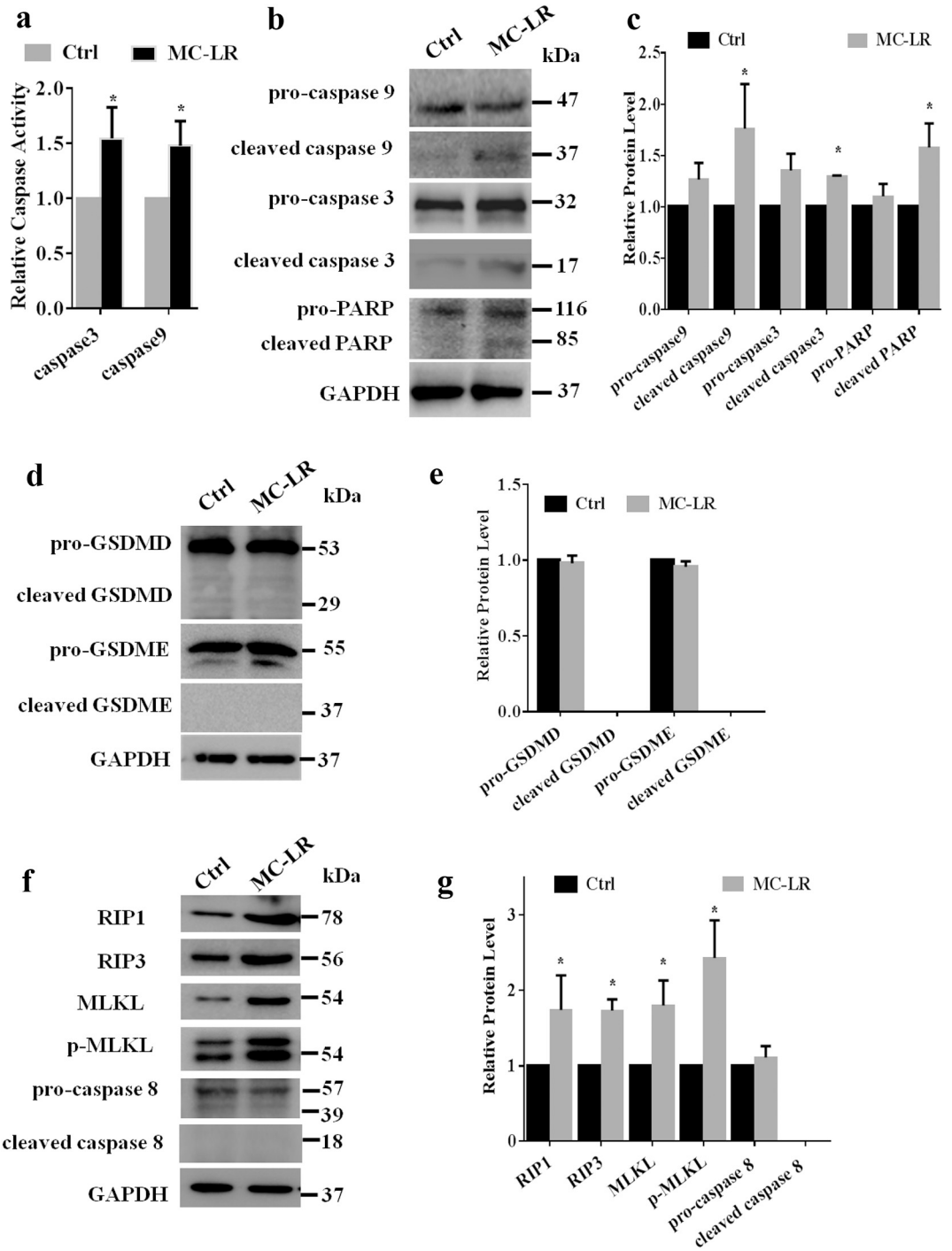

Fig. 2. Screening of biochemical markers in MC-LR-treated primary mouse hepatocytes.
(a–c) Apoptotic caspases and PARP were detected in MC-LR-treated or control cells. The activities of caspase-9 and caspase-3 are measured and shown (a). Cleavage of caspase-9, caspase-3 and PARP in MC-LR-treated cells or control cells was detected (b and c). (d–e) MCLR-induced cleavage of the pyroptotic proteins GSDMD and GSDME was assessed by western blot analysis. (f and g) Necroptotic RIP1, RIP3, and MLKL expression, MLKL phosphorylation and caspase-8 cleavage were also detected. DMEM treatment served as the negative control. GAPDH served as a loading control for western blot analysis. Results are shown as the mean ± S.D. values from three separate experiments performed in duplicate. *$p < .05$ versus the control cells.

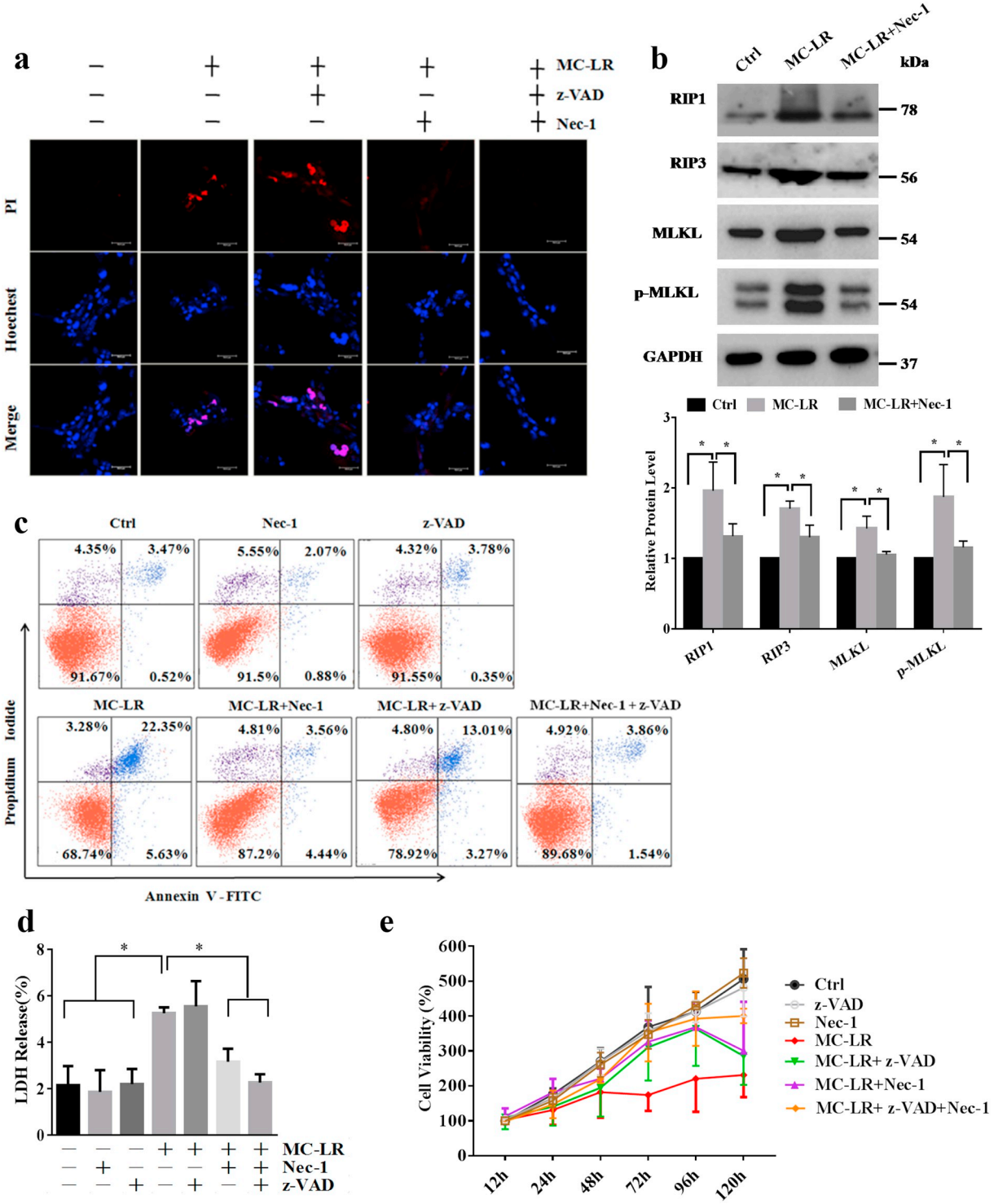

Fig. 3. MC-LR-induced necroptotic death of primary mouse hepatocytes.
Primary mouse hepatocytes were treated with or without different inhibitors, including zVAD (5 μm z-VAD-fmk, a pan-caspase inhibitor) and nec-1 (8 μm necrostatin-1, a specific inhibitor of RIP1), for 1 h, and this was followed by MC-LR treatment to evaluate the necroptotic features. (a) Representative confocal imaging of cells treated with the indicated treatments. Cells were harvested at 48 h after MC-LR treatment, stained with PI and analyzed by confocal microscopy. Nuclei were counterstained with Hoechst 33242 (blue). (b) Comparison of RIP1, RIP3, and MLKL expression and MLKL phosphorylation of cells with the indicated treatments. (c) Flow cytometry analysis of PI- and annexin V–FITC-stained cells subjected to the indicated treatments. (d and e) Comparison of cell viability and LDH release in cells subjected to the indicated treatments. Results are shown as the mean ± S.D. values of three separate experiments performed in duplicate. *p < .05 versus the control cells. (For interpretation of the references to colour in this figure legend, the reader is referred to the web version of this article.)

et al., 2017), GSTT2 (Schlormann et al., 2017), UCP2 (Pecqueur et al., 2001), NQO1 (Wu et al., 2013), NOX4 (Lener et al., 2009), GCLC (Sikalidis et al., 2014), NOS3 (Zhen et al., 2008), MAOA (Kaludercic et al., 2010), GPX1 (Ardanaz et al., 2010), and GPX3 (Jin et al., 2011), as shown in Table 2] was determined in MC-LR-treated cells and control cells. Real-time RT-PCR (Fig. 5d) and western blot analysis (Fig. 5e and

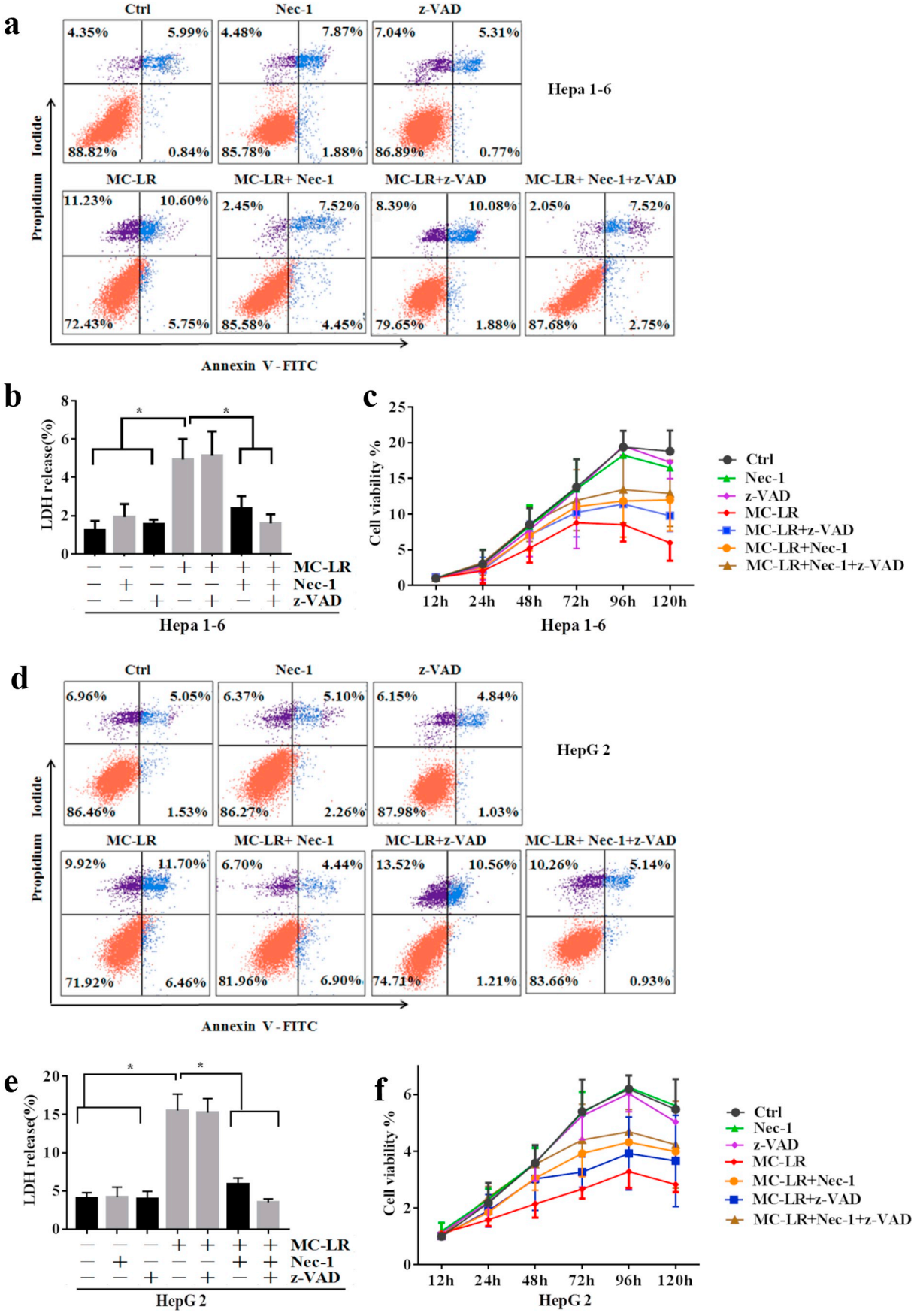

Fig. 4. MC-LR-induced necroptotic death of hepatoma cell lines.
(a–c) Flow cytometry analysis, cell viability and LDH release assays subjected to the indicated treatments in mouse hepatoma cell line Hepa 1–6. (d–f) Flow cytometry analysis, cell viability and LDH release assays subjected to the indicated treatments in human hepatoma cell line HepG2. Results are shown as the mean ± S.D. values of three separate experiments performed in duplicate. *$p < .05$ versus the control cells.

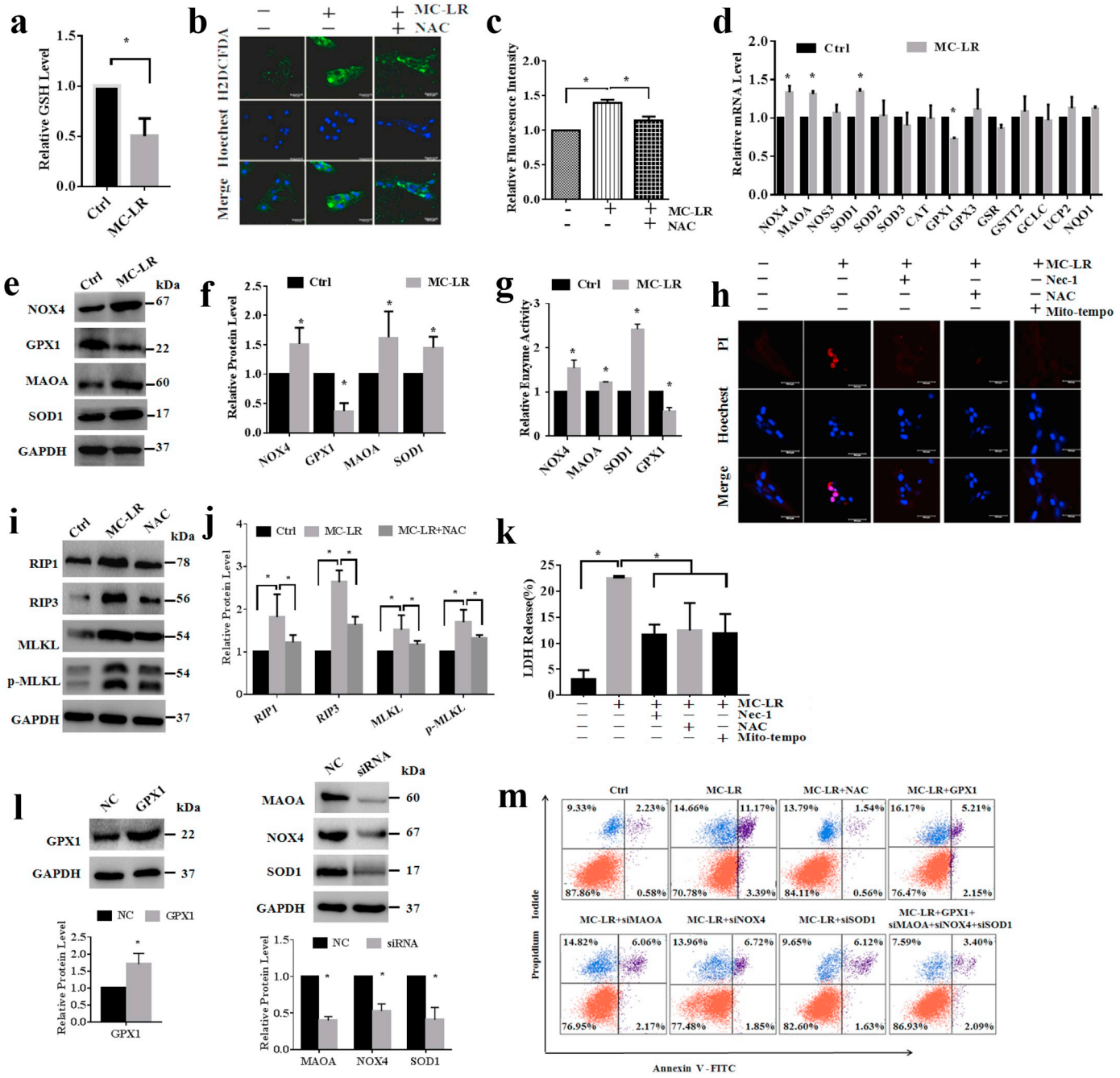

Fig. 5. Involvement of the ROS pathway in necroptosis induced by MC-LR.

Primary mouse hepatocytes were treated with or without different inhibitors, including NAC (5 mM N-Acetyl-L-cysteine, a total ROS scavenger), nec-1 (8 μm necrostatin-1, a specific inhibitor of RIP1), or Mito-tempo (3 μM, an mtROS scavenger), and this was followed by MC-LR treatment to detect the ROS level or to evaluate the necroptotic features. (a) MC-LR treatment resulted in a decrease in the GSH levels. GSH content was measured in MC-LR-treated or control cell lysates using a glutathione assay kit, as described under Materials and Methods. (b and c) Effect of MC-LR on ROS generation in cells subjected to the indicated treatments. Intracellular ROS appeared green under a fluorescent microscope, and the green fluorescent intensity was quantified. (d–f) Effects of MC-LR on the mRNA and protein levels of the pro-oxidant/antioxidant enzymes. (g) The effects of MC-LR on SOD1, MAOA, NOX4 and GPX1 enzymatic activity were assayed spectrophotometrically. (h) Representative confocal imaging of cells subjected to the indicated treatments. Cells were harvested at 48 h after MC-LR treatment, stained with PI, and analyzed by confocal microscopy. (i and j) Comparison of RIP1, RIP3, and MLKL expression and MLKL phosphorylation of cells with the indicated treatments. (k) Comparison of LDH release in cells subjected to the indicated treatments. (l and m) Effects of either over-expression of GPX1 or knockdown of MAOA, NOX4 and SOD1. Results are shown as the mean ± S.D. values from three separate experiments performed in duplicate. *$p < .05$ versus the control cells. (For interpretation of the references to colour in this figure legend, the reader is referred to the web version of this article.)

f) revealed that the expression levels of the pro-oxidant enzymes SOD1, MAOA, and NOX4 in the groups exposed to MC-LR were significantly elevated, while the level of the antioxidant GPX1 was significantly decreased by MC-LR treatment. With regard to their enzymatic activity, as shown in Fig. 5g, MC-LR treatment significantly induced the activity of the pro-oxidants SOD1, MAOA, and NOX4 but reduced the activity of the antioxidant GPX1. Thus, the expression levels and functional activity of these enzymes showed good correlation. These data indicate that the dysregulation of the pro-oxidant/antioxidant balance by MC-LR treatment resulted in an imbalance in the dynamic balance between

Table 2
14 pro-oxidant/antioxidant enzymes.

Enzymes	Aliases	Functions	Reference
CAT	Catalase,cas-1	Encode catalase, a key antioxidant enzyme defense against oxidative stress	[Deng et al., 2012; Yabe et al., 2002]
SOD1	SOD; Cu/Zn Superoxide Dismutase	Destroy intracellular radicals	[Iuchi et al., 2007]
SOD2	Mn-SOD	Destroy superoxide anion radicals from mitochondria	[Hosoki et al., 2012]
SOD3	Extracellular Superoxide Dismutase [Cu−Zn]	Convert extracellular superoxide radicals into hydrogen peroxide and oxygen	[Kwon et al., 2015]
GSR	GR,GR1	Reduce oxidized glutathione disulfide (GSSG) to the sulfhydryl form GSH, an important antioxidant	[Han et al., 2017]
GSTT2	GST Class-Theta-2	Catalyze the conjugation of reduced glutathione to a variety of electrophilic and hydrophobic compounds	[Schlormann et al., 2017]
UCP2	SLC25A8, UCPH	Regulate the production of reactive oxygen species from mitochondria	[Pecqueur et al., 2001]
MAOA	Amine Oxidase A	Catalyze the oxidative deamination of biogenic and xenobiotic amines, generating hydrogen peroxide	[Kaludercic et al., 2010]
NOS3	eNOS, Endothelial NOS	A reactive free radicals, strongly susceptible to upregulation by ROS	[Zhen et al., 2008]
NOX4	KOX-1	Catalyze the production of reactive oxygen species	[Lener et al., 2009]
GCLC	GLCL-H; Ggcs-hs	A rate-limiting enzyme of GSH biosynthetic pathway	[Sikalidis et al., 2014]
NQO1	NAD(P)H Quinone Dehydrogenase 1	Prevent the one electron reduction of quinones that results in the production of radical species	[Wu et al., 2013]
GPX1	GSHPX1,GPXD	Convert hydrogen peroxide and organic hydroperoxides to nonreactive products	[Ardanaz et al., 2010
GPX3	GSHPx-3,GPXP	Plasma antioxidant enzyme, inactivate ROS	[Jin et al., 2011]

ROS production and elimination in hepatocytes. Moreover, as indicated in Fig. 5h, treatment with MC-LR enhanced the number of PI+ cells, which is indicative of cell death. However, *N*-acetyl-L-cysteine (NAC) and mito-tempo, which are inhibitors of ROS, markedly attenuated the MC-LR-induced ROS elevation, thereby rescuing cell death. Nec-1 was also used as a positive control. Expectedly, NAC also inhibited the expression of RIP1, RIP3, MLKL, and p-MLKL (Fig. 5i and j), as well as LDH release (Fig. 5 k). In addition, we further examined and compared the levels of apoptosis and necroptosis by Annexin-V/PI dual staining for flow cytometric analysis, in the control and MCLR-treated cells without or with the treatments by NAC, GPX1 over-expression, RNA interference of MAOA, NOX4 or SOD1. NAC was also used as a positive control. As shown in Fig. 5I and m, a dramatic increase in the percentage of Annexin-V-FITC(+)/PI(−) cells (lower right quadrant) and Annexin-V-FITC(+)/PI(+) cells (upper right quadrant) were observed in the MCLR-treated cells, indicating that MC-LR increased apoptotic and necroptotic susceptibility of the cells. Either over-expression of GPX1, or knockdown of MAOA, NOX4 or SOD1 moderately reduced the percentage of the early apoptotic cells and necroptotic cells. But they were more effective when used in combination than when used individually. These findings indicate that MC-LR induced necroptosis in an ROS-dependent manner in primary mouse hepatocytes.

4. Discussion

In the present study, we demonstrate that MC-LR, which has so far been reported only in association with apoptosis, can induce another type of programmed cell death—necroptosis—in primary mouse hepatocytes.

Due to its high molecular weight (varying from 900 to 1100 Da), MC-LR is taken up by hepatocytes via the organic anion transporter polypeptides 1B1 (OATP1B1) and OATP1B3 (Eriksson et al., 1990; Fischer et al., 2005; Runnegar et al., 1995). Primary hepatocytes better simulate the in vivo conditions, have higher OATP expression, and are more susceptible to MCLR-induced cytotoxicity (Fischer et al., 2010; Ulvestad et al., 2012). This was also proved by our present study, as indicated in Fig. 3 and Fig. 4, primary cultured mouse hepatocytes are more susceptible to MCLR-induced cytotoxicity (< 10 nM) than hepatoma cell lines (20 μM for HepG2 and 10 μM for Hepa 1–6). Thus, in the present study, primary cultured mouse hepatocytes isolated by optimized in situ perfusion methods were chosen as the in vitro model to investigate the toxic effects of MC-LR. MC-LR has been shown to induce programmed cell death in the form of apoptosis, but we wanted to investigate the potential involvement of necroptosis and pyroptosis as programmed cell pathways too. Annexin V/PI dual staining with flow cytometric analysis showed that the MC-LR-treated primary mouse hepatocytes had a considerably lower cell viability rate than the control cells and also exhibited significant LDH release (which is indicative of plasma membrane rupture). In particular, the staining data and patterns indicated the presence of necroptotic cells, as demonstrated by the presence of PI-stained cells. These data indicate that MC-LR may induce lytic programmed cell death through pathways other than apoptosis.

In order to determine which pathways are associated with MC-LR-induced cell death, western blot analysis was used to detect the expression of key players associated with necroptotis and pyroptotis (Fig. 2). MC-LR-treated cells showed significantly upregulated expression of the necroptotic proteins RIP1, RIP3, MLKL and p-MLKL, but no marked cleavage of pyroptotic GSDMD and GSDME was observed. Furthermore, the necroptotic inhibitor nec-1 was found to remarkably attenuate the number of PI+ cells, but it did not affect the number of apoptotic cells. In contrast, the apoptotic inhibitor zVAD only downregulated the annexin V–FITC+ cells and did not affect the necroptotic cells. Thus, nec-1 and zVAD could inhibit necroptosis and apoptosis, respectively, but they were more effective in treating MCLR-induced cell injury when used in combination than when used individually (Fig. 3 and Fig. 4). These results indicate that MC-LR treatment induced both apoptosis and necroptosis, which coexisted in a relatively independent way, in the primary cultured mouse hepatocytes. Previous studies have reported that activation of necroptosis is a pathophysiological event in chronic inflammatory liver diseases, namely, alcoholic and non-alcoholic steatohepatitis (Afonso et al., 2015; Gautheron et al., 2014; Roychowdhury et al., 2013). Further, necroptosis has also been suggested to mediate experimental acetaminophen-induced hepatotoxicity in early phases, although the findings are controversial (Deutsch et al., 2015; Ramachandran et al., 2013; Yang et al., 2016) Further, p-MLKL has been detected in liver biopsy samples from patients with drug-induced liver injury (Wang et al., 2014). These findings indicate that there might exist some crosstalk between apoptosis and necroptosis as MC-LR treatment progresses; these pathways therefore need further investigation.

Necroptosis plays a role in a wide range of pathological cell death events, such as ischemic brain injury, myocardial infarction, excitotoxicity and chemotherapy-induced cell death (Vandenabeele et al., 2008). ROS have long been considered a driving force for necroptosis. In particular, oxidation of specific cysteins in RIP1 by ROS leads to necrosome activation (Yang et al., 2018). It has been reported that RIP3-induced mitochondrial ROS production leads to necroptosis in response to TNF-α stimulation (Yang et al., 2018; Zhang et al., 2009).

Previous studies have indicated that MC-LR exposure could lead to oxidative stress in cells and induce apoptosis or cell death (Chen and Xie, 2016; Kleppe et al., 2015). As shown in our results (Fig. 5), gradual elevation in ROS production was observed in hepatocytes exposed to MC-LR, in accordance with previous studies (Huang et al., 2015). Our study showed that MCLR-induced ROS overgeneration results in the dysregulation of the pro-oxidants SOD1, MAOA, and NOX4 and the antioxidant GPX1. Similarly, the involvement of NOX1 in necroptosis has also been reported by Kim et al. (2007). NAC and mito-tempo treatment, GPX1 over-expression, MAOA, NOX4 and SOD1 knockdown effectively reduced ROS accumulation and thereby rescued MCLR-induced necroptosis; this indicates that ROS signaling plays a causative role in MCLR-induced cell death and hepatotoxicity. However, there is some controversy with regard to the role of ROS in cell death. For instance, some publications have indicated that modest amounts of ROS can induce apoptosis, whereas necroptosis occurs when cells of a similar type are exposed to high ROS levels (Saito et al., 2006; Takeda et al., 1999; Teramoto et al., 1999). Therefore, ROS may play various roles in cell death, for example, by directly oxidizing cellular components and by initiating cell death through the activation of relevant signaling pathways.

In summary, our study confirms that necroptosis occurs in MC-LR-treated primary mouse hepatocytes. Further, the findings indicate that MC-LR induces both apoptosis and necroptosis in this cell line, and these processes appear to take place concurrently and independently of each other. With regard to the involved molecules, it seems that ROS acts as a causative factor for MC-LR-driven necroptosis. Thus, our study demonstrates that MCLR-induced necroptosis is a novel target in the treatment of patients exposed to MC-LR.

Acknowledgements

We are grateful to Mr. Zhi-hong Huang and Jun-jin Lin (Fujian Medical University, Fuzhou, China) for their excellent technical assistance. This work was supported by grants from the Natural Science Foundation of Fujian province (No. 2016J01365), the Training Program Foundation for Middle-aged and Young Talents from Sanitation System of Fujian Province (2016-ZQN-66), the Joint Funds for the Innovation of Science and Technology, Fujian Province (No. 2016Y9035), and Program for New Century Excellent Talents in Fujian Province University (No. 2018B027).

Conflicts of interest

The authors have no conflicts of interest to declare.

References

Afonso, M.B., Rodrigues, P.M., Carvalho, T., Caridade, M., Borralho, P., Cortez-Pinto, H., Castro, R.E., Rodrigues, C.M., 2015. Necroptosis is a key pathogenic event in human and experimental murine models of non-alcoholic steatohepatitis. Clin. Sci. (Lond.) 129 (8), 721–739.

Amado, L.L., Monserrat, J.M., 2010. Oxidative stress generation by microcystins in aquatic animals: why and how. Environ. Int. 36 (2), 226–235.

Ardanaz, N., Yang, X.P., Cifuentes, M.E., Haurani, M.J., Jackson, K.W., Liao, T.D., Carretero, O.A., Pagano, P.J., 2010. Lack of glutathione peroxidase 1 accelerates cardiac-specific hypertrophy and dysfunction in angiotensin II hypertension. Hypertension 55 (1), 116–123.

Bischoff, K., 2001. The toxicology of microcystin-LR: occurrence, toxicokinetics, toxicodynamics, diagnosis and treatment. Vet. Hum. Toxicol. 43 (5), 294–297.

Cai, Z., Jitkaew, S., Zhao, J., Chiang, H.C., Choksi, S., Liu, J., Ward, Y., Wu, L.G., Liu, Z.G., 2014. Plasma membrane translocation of trimerized MLKL protein is required for TNF-induced necroptosis. Nat. Cell Biol. 16 (1), 55–65.

Campos, A., Vasconcelos, V., 2010. Molecular mechanisms of microcystin toxicity in animal cells. Int. J. Mol. Sci. 11 (1), 268–287.

Chen, L., Xie, P., 2016. Mechanisms of microcystin-induced cytotoxicity and apoptosis. Mini. Rev. Med. Chem. 16 (13), 1018–1031.

Cho, Y.S., Challa, S., Moquin, D., Genga, R., Ray, T.D., Guildford, M., Chan, F.K., 2009. Phosphorylation-driven assembly of the RIP1-RIP3 complex regulates programmed necrosis and virus-induced inflammation. Cell 137 (6), 1112–1123.

Cho, Y., Challa, S., Chan, F.K., 2011. A RNA interference screen identifies RIP3 as an essential inducer of TNF-induced programmed necrosis. Adv. Exp. Med. Biol. 691, 589–593.

Deng, X., Wu, K., Wan, J., Li, L., Jiang, R., Jia, M., Jing, Y., Zhang, L., 2012. Aminotriazole attenuated carbon tetrachloride-induced oxidative liver injury in mice. Food Chem. Toxicol. 50 (9), 3073–3078.

Deutsch, M., Graffeo, C.S., Rokosh, R., Pansari, M., Ochi, A., Levie, E.M., Van Heerden, E., Tippens, D.M., Greco, S., Barilla, R., et al., 2015. Divergent effects of RIP1 or RIP3 blockade in murine models of acute liver injury. Cell Death Dis. 6, e1759.

Ding, W.X., Shen, H.M., Ong, C.N., 2000. Critical role of reactive oxygen species and mitochondrial permeability transition in microcystin-induced rapid apoptosis in rat hepatocytes. Hepatology 32 (3), 547–555.

Ding, J., Wang, K., Liu, W., She, Y., Sun, Q., Shi, J., Sun, H., Wang, D.C., Shao, F., 2016. Pore-forming activity and structural autoinhibition of the gasdermin family. Nature 535 (7610), 111–116.

Dixon, S.J., Stockwell, B.R., 2014. The role of iron and reactive oxygen species in cell death. Nat. Chem. Biol. 10 (1), 9–17.

Dondelinger, Y., Aguileta, M.A., Goossens, V., Dubuisson, C., Grootjans, S., Dejardin, E., Vandenabeele, P., Bertrand, M.J., 2013. RIPK3 contributes to TNFR1-mediated RIPK1 kinase-dependent apoptosis in conditions of cIAP1/2 depletion or TAK1 kinase inhibition. Cell Death Differ. 20 (10), 1381–1392.

Eriksson, J.E., Gronberg, L., Nygard, S., Slotte, J.P., Meriluoto, J.A., 1990. Hepatocellular uptake of 3H-dihydromicrocystin-LR, a cyclic peptide toxin. Biochim. Biophys. Acta 1025 (1), 60–66.

Falconer, I.R., Humpage, A.R., 2005. Health risk assessment of cyanobacterial (blue-green algal) toxins in drinking water. Int. J. Environ. Res. Public Health 2 (1), 43–50.

Fischer, W.J., Altheimer, S., Cattori, V., Meier, P.J., Dietrich, D.R., Hagenbuch, B., 2005. Organic anion transporting polypeptides expressed in liver and brain mediate uptake of microcystin. Toxicol. Appl. Pharmacol. 203 (3), 257–263.

Fischer, A., Hoeger, S.J., Stemmer, K., Feurstein, D.J., Knobeloch, D., Nussler, A., Dietrich, D.R., 2010. The role of organic anion transporting polypeptides (OATPs/SLCOs) in the toxicity of different microcystin congeners in vitro: a comparison of primary human hepatocytes and OATP-transfected HEK293 cells. Toxicol. Appl. Pharmacol. 245 (1), 9–20.

Fladmark, K.E., Brustugun, O.T., Hovland, R., Boe, R., Gjertsen, B.T., Zhivotovsky, B., Doskeland, S.O., 1999. Ultrarapid caspase-3 dependent apoptosis induction by serine/threonine phosphatase inhibitors. Cell Death Differ. 6 (11), 1099–1108.

Gates, A.J., Hughes, R.O., Sharp, S.R., Millington, P.D., Nilavongse, A., Cole, J.A., Leach, E.R., Jepson, B., Richardson, D.J., Butler, C.S., 2003. Properties of the periplasmic nitrate reductases from Paracoccus pantotrophus and Escherichia coli after growth in tungsten-supplemented media. FEMS Microbiol. Lett. 220 (2), 261–269.

Gautheron, J., Vucur, M., Reisinger, F., Cardenas, D.V., Roderburg, C., Koppe, C., Kreggenwinkel, K., Schneider, A.T., Bartneck, M., Neumann, U.P., et al., 2014. A positive feedback loop between RIP3 and JNK controls non-alcoholic steatohepatitis. EMBO Mol. Med. 6 (8), 1062–1074.

Gehringer, M.M., 2004. Microcystin-LR and okadaic acid-induced cellular effects: a dualistic response. FEBS Lett. 557 (1–3), 1–8.

Han, C., Kim, M.J., Ding, D., Park, H.J., White, K., Walker, L., Gu, T., Tanokura, M., Yamasoba, T., Linser, P., et al., 2017. GSR is not essential for the maintenance of antioxidant defenses in mouse cochlea: possible role of the thioredoxin system as a functional backup for GSR. PLoS One 12 (7), e0180817.

Hosoki, A., Yonekura, S., Zhao, Q.L., Wei, Z.L., Takasaki, I., Tabuchi, Y., Wang, L.L., Hasuike, S., Nomura, T., Tachibana, A., et al., 2012. Mitochondria-targeted superoxide dismutase (SOD2) regulates radiation resistance and radiation stress response in HeLa cells. J. Radiat. Res. 53 (1), 58–71.

Huang, X., Chen, L., Liu, W., Qiao, Q., Wu, K., Wen, J., Huang, C., Tang, R., Zhang, X., 2015. Involvement of oxidative stress and cytoskeletal disruption in microcystin-induced apoptosis in CIK cells. Aquat. Toxicol. 165, 41–50.

Iuchi, Y., Okada, F., Onuma, K., Onoda, T., Asao, H., Kobayashi, M., Fujii, J., 2007. Elevated oxidative stress in erythrocytes due to a SOD1 deficiency causes anaemia and triggers autoantibody production. Biochem. J. 402 (2), 219–227.

Jayaraj, R., Anand, T., Rao, P.V., 2006. Activity and gene expression profile of certain antioxidant enzymes to microcystin-LR induced oxidative stress in mice. Toxicology 220 (2–3), 136–146.

Jia, J., Luo, W., Lu, Y., Giesy, J.P., 2014. Bioaccumulation of microcystins (MCs) in four fish species from Lake Taihu, China: assessment of risks to humans. Sci. Total Environ. 487, 224–232.

Jin, R.C., Mahoney, C.E., Coleman Anderson, L., Ottaviano, F., Croce, K., Leopold, J.A., Zhang, Y.Y., Tang, S.S., Handy, D.E., Loscalzo, J., 2011. Glutathione peroxidase-3 deficiency promotes platelet-dependent thrombosis in vivo. Circulation 123 (18), 1963–1973.

Kaludercic, N., Takimoto, E., Nagayama, T., Feng, N., Lai, E.W., Bedja, D., Chen, K., Gabrielson, K.L., Blakely, R.D., Shih, J.C., et al., 2010. Monoamine oxidase A-mediated enhanced catabolism of norepinephrine contributes to adverse remodeling and pump failure in hearts with pressure overload. Circ. Res. 106 (1), 193–202.

Kim, Y.S., Morgan, M.J., Choksi, S., Liu, Z.G., 2007. TNF-induced activation of the Nox1 NADPH oxidase and its role in the induction of necrotic cell death. Mol. Cell 26 (5), 675–687.

Kleppe, R., Herfindal, L., Doskeland, S.O., 2015. Cell death inducing microbial protein phosphatase inhibitors—mechanisms of action. Mar. Drugs 13 (10), 6505–6520.

Komatsu, M., Furukawa, T., Ikeda, R., Takumi, S., Nong, Q., Aoyama, K., Akiyama, S., Keppler, D., Takeuchi, T., 2007. Involvement of mitogen-activated protein kinase signaling pathways in microcystin-LR-induced apoptosis after its selective uptake mediated by OATP1B1 and OATP1B3. Toxicol. Sci. 97 (2), 407–416.

Kwon, M.J., Lee, K.Y., Lee, H.W., Kim, J.H., Kim, T.Y., 2015. SOD3 variant, R213G, altered SOD3 function, leading to ROS-mediated inflammation and damage in multiple organs of premature aging mice. Antioxid. Redox Signal. 23 (12), 985–999.

Lener, B., Koziel, R., Pircher, H., Hutter, E., Greussing, R., Herndler-Brandstetter, D., Hermann, M., Unterluggauer, H., Jansen-Durr, P., 2009. The NADPH oxidase Nox4 restricts the replicative lifespan of human endothelial cells. Biochem. J. 423 (3), 363–374.

Lone, Y., Bhide, M., Koiri, R.K., 2017. Amelioratory effect of coenzyme Q10 on potential human carcinogen microcystin-LR induced toxicity in mice. Food Chem. Toxicol. 102, 176–185.

Newton, K., Dugger, D.L., Wickliffe, K.E., Kapoor, N., de Almagro, M.C., Vucic, D., Komuves, L., Ferrando, R.E., French, D.M., Webster, J., et al., 2014. Activity of protein kinase RIPK3 determines whether cells die by necroptosis or apoptosis. Science 343 (6177), 1357–1360.

Pecqueur, C., Alves-Guerra, M.C., Gelly, C., Levi-Meyrueis, C., Couplan, E., Collins, S., Ricquier, D., Bouillaud, F., Miroux, B., 2001. Uncoupling protein 2, in vivo distribution, induction upon oxidative stress, and evidence for translational regulation. J. Biol. Chem. 276 (12), 8705–8712.

Pouria, S., de Andrade, A., Barbosa, J., Cavalcanti, R.L., Barreto, V.T., Ward, C.J., Preiser, W., Poon, G.K., Neild, G.H., Codd, G.A., 1998. Fatal microcystin intoxication in haemodialysis unit in Caruaru, Brazil. Lancet 352 (9121), 21–26.

Ramachandran, A., McGill, M.R., Xie, Y., Ni, H.M., Ding, W.X., Jaeschke, H., 2013. Receptor interacting protein kinase 3 is a critical early mediator of acetaminophen-induced hepatocyte necrosis in mice. Hepatology 58 (6), 2099–2108.

Roychowdhury, S., McMullen, M.R., Pisano, S.G., Liu, X., Nagy, L.E., 2013. Absence of receptor interacting protein kinase 3 prevents ethanol-induced liver injury. Hepatology 57 (5), 1773–1783.

Runnegar, M., Berndt, N., Kaplowitz, N., 1995. Microcystin uptake and inhibition of protein phosphatases: effects of chemoprotectants and self-inhibition in relation to known hepatic transporters. Toxicol. Appl. Pharmacol. 134 (2), 264–272.

Saito, Y., Nishio, K., Ogawa, Y., Kimata, J., Kinumi, T., Yoshida, Y., Noguchi, N., Niki, E., 2006. Turning point in apoptosis/necrosis induced by hydrogen peroxide. Free Radic. Res. 40 (6), 619–630.

Schieber, M., Chandel, N.S., 2014. ROS function in redox signaling and oxidative stress. Curr. Biol. 24 (10), R453–R462.

Schlormann, W., Lamberty, J., Ludwig, D., Lorkowski, S., Glei, M., 2017. In vitro-fermented raw and roasted walnuts induce expression of CAT and GSTT2 genes, growth inhibition, and apoptosis in LT97 colon adenoma cells. Nutr. Res. 47, 72–80.

Shammo, J.M., Stein, B.L., 2016. Mutations in MPNs: prognostic implications, window to biology, and impact on treatment decisions. Hematol. Am. Soc. Hematol. Educ. Program 2016 (1), 552–560.

Shi, J., Zhao, Y., Wang, K., Shi, X., Wang, Y., Huang, H., Zhuang, Y., Cai, T., Wang, F., Shao, F., 2015. Cleavage of GSDMD by inflammatory caspases determines pyroptotic cell death. Nature 526 (7575), 660–665.

Shuai, Y., Lou, D., Yin, J., Qian, X., Wang, Y., Hong, X., Xiao, P., Zhong, W., 2017. Characterization of microcystin-induced dualistic toxic effects on primary rat hepatocytes. J. Environ. Pathol. Toxicol. Oncol. 36 (1), 15–27.

Sikalidis, A.K., Mazor, K.M., Lee, J.I., Roman, H.B., Hirschberger, L.L., Stipanuk, M.H., 2014. Upregulation of capacity for glutathione synthesis in response to amino acid deprivation: regulation of glutamate-cysteine ligase subunits. Amino Acids 46 (5), 1285–1296.

Soares, R.M., Yuan, M., Servaites, J.C., Delgado, A., Magalhaes, V.F., Hilborn, E.D., Carmichael, W.W., Azevedo, S.M., 2006. Sublethal exposure from microcystins to renal insufficiency patients in Rio de Janeiro, Brazil. Environ. Toxicol. 21 (2), 95–103.

Song, L., Chen, W., Peng, L., Wan, N., Gan, N., Zhang, X., 2007. Distribution and bioaccumulation of microcystins in water columns: a systematic investigation into the environmental fate and the risks associated with microcystins in Meiliang Bay, Lake Taihu. Water Res. 41 (13), 2853–2864.

Sun, L., Wang, H., Wang, Z., He, S., Chen, S., Liao, D., Wang, L., Yan, J., Liu, W., Lei, X., et al., 2012. Mixed lineage kinase domain-like protein mediates necrosis signaling downstream of RIP3 kinase. Cell 148 (1–2), 213–227.

Takeda, M., Shirato, I., Kobayashi, M., Endou, H., 1999. Hydrogen peroxide induces necrosis, apoptosis, oncosis and apoptotic oncosis of mouse terminal proximal straight tubule cells. Nephron 81 (2), 234–238.

Takumi, S., Komatsu, M., Furukawa, T., Ikeda, R., Sumizawa, T., Akenaga, H., Maeda, Y., Aoyama, K., Arizono, K., Ando, S., et al., 2010. p53 plays an important role in cell fate determination after exposure to microcystin-LR. Environ. Health Perspect. 118 (9), 1292–1298.

Teramoto, S., Tomita, T., Matsui, H., Ohga, E., Matsuse, T., Ouchi, Y., 1999. Hydrogen peroxide-induced apoptosis and necrosis in human lung fibroblasts: protective roles of glutathione. Jpn. J. Pharmacol. 79 (1), 33–40.

Ulvestad, M., Darnell, M., Molden, E., Ellis, E., Asberg, A., Andersson, T.B., 2012. Evaluation of organic anion-transporting polypeptide 1B1 and CYP3A4 activities in primary human hepatocytes and HepaRG cells cultured in a dynamic three-dimensional bioreactor system. J. Pharmacol. Exp. Ther. 343 (1), 145–156.

Vandenabeele, P., Declercq, W., Vanden Berghe, T., 2008. Necrotic cell death and 'necrostatins': now we can control cellular explosion. Trends Biochem. Sci. 33 (8), 352–355.

Vince, J.E., Wong, W.W., Gentle, I., Lawlor, K.E., Allam, R., O'Reilly, L., Mason, K., Gross, O., Ma, S., Guarda, G., et al., 2012. Inhibitor of apoptosis proteins limit RIP3 kinase-dependent interleukin-1 activation. Immunity 36 (2), 215–227.

Wang, H., Sun, L., Su, L., Rizo, J., Liu, L., Wang, L.F., Wang, F.S., Wang, X., 2014. Mixed lineage kinase domain-like protein MLKL causes necrotic membrane disruption upon phosphorylation by RIP3. Mol. Cell 54 (1), 133–146.

Wang, Y., Gao, W., Shi, X., Ding, J., Liu, W., He, H., Wang, K., Shao, F., 2017. Chemotherapy drugs induce pyroptosis through caspase-3 cleavage of a gasdermin. Nature 547 (7661), 99–103.

Wu, Y.L., Wang, D., Peng, X.E., Chen, Y.L., Zheng, D.L., Chen, W.N., Lin, X., 2013. Epigenetic silencing of NAD(P)H:quinone oxidoreductase 1 by hepatitis B virus X protein increases mitochondrial injury and cellular susceptibility to oxidative stress in hepatoma cells. Free Radic. Biol. Med. 65, 632–644.

Yabe, Y., Kobayashi, N., Nishikawa, M., Mihara, K., Yamashita, F., Takakura, Y., Hashida, M., 2002. Pharmacokinetics and preventive effects of targeted catalase derivatives on hydrogen peroxide-induced injury in perfused rat liver. Pharm. Res. 19 (12), 1815–1821.

Yang, X., Chao, X., Wang, Z.T., Ding, W.X., 2016. The end of RIPK1-RIPK3-MLKL-mediated necroptosis in acetaminophen-induced hepatotoxicity? Hepatology 64 (1), 311–312.

Yang, Z., Wang, Y., Zhang, Y., 2018. RIP3 Targets Pyruvate Dehydrogenase Complex to Increase Aerobic Respiration in TNF-induced Necroptosis. 20(2). pp. 186–197.

Zegura, B., Straser, A., Filipic, M., 2011. Genotoxicity and potential carcinogenicity of cyanobacterial toxins - a review. Mutat. Res. 727 (1–2), 16–41.

Zhang, D.W., Shao, J., Lin, J., Zhang, N., Lu, B.J., Lin, S.C., Dong, M.Q., Han, J., 2009. RIP3, an energy metabolism regulator that switches TNF-induced cell death from apoptosis to necrosis. Science 325 (5938), 332–336.

Zhang, Y., Chen, X., Gueydan, C., Han, J., 2018. Plasma membrane changes during programmed cell deaths. Cell Res. 28 (1), 9–21.

Zhen, J., Lu, H., Wang, X.Q., Vaziri, N.D., Zhou, X.J., 2008. Upregulation of endothelial and inducible nitric oxide synthase expression by reactive oxygen species. Am. J. Hypertens. 21 (1), 28–34.